Journal of Physics:
Conference Series

PURPOSE-LED
PUBLISHING™

PAPER • **OPEN ACCESS**

Effect of oxygen stoichiometry on the energy of CEF levels in $Pr_2NiO_{4.25}$

To cite this article: Laura Zeni Cunha *et al* 2026 *J. Phys.: Conf. Ser.* **3161** 012020

View the article online for updates and enhancements.

You may also like

- Crystal-field interactions in $PrRu_2Si_2$
R Michalski, Z Ropka and R J Radwanski
- Magnetic ground state of Pr in $(Pr_{1.5}Ce_{0.5})Sr_2Cu_2NbO_{10-\delta}$
U Staub, L Soderholm, R Osborn et al.
- Magnetism in praseodymium-neodymium single-crystal alloys
B Lebech, K A McEwen and P A Lindgard

This content was downloaded from IP address 134.130.185.46 on 25/08/2026 at 07:00

Journal of Physics: Conference Series **3161** (2026) 012020 doi:10.1088/1742-6596/3161/1/012020

Effect of oxygen stoichiometry on the energy of CEF levels in $Pr_2NiO_{4.25}$

Laura Zeni Cunha[1,2], Andrea Piovano[1*], Martin Boehm[1], Monica Ceretti[2], Wolfgang Schmidt[3], Martin Meven[4,5], Werner Paulus[2]

[1] Institut Laue-Langevin (ILL), 71 Avenue des Martyrs, 38042 Grenoble, France
[2] ICGM, Univ. Montpellier, CNRS, ENSCM, Montpellier 34000, France
[3] Forschungszentrum Jülich GmbH, Jülich Centre for Neutron Science at ILL, 71 Avenue des Martyrs, 38042 Grenoble, France
[4] Jülich Centre for Neutron Science (JCNS) at Heinz Maier-Leibnitz Zentrum (MLZ), Forschungszentrum Jülich GmbH, Lichtenbergstrasse 1, 85747 Garching, Germany
[5] Institute of Crystallography, RWTH Aachen University, 52056 Aachen, Germany

[*]E-mail: piovano@ill.fr

Abstract. In this work, we present a study of the CEF environment in $Pr_2NiO_{4+\delta}$ (δ = 0.25), through the analysis of inelastic neutron scattering measurements combined with point charge model simulations. Inelastic neutron scattering experiments on $Pr_2NiO_{4.25}$ were conducted using the thermal triple-axis spectrometer IN20 at the Institut Laue-Langevin. An inelastic peak was observed at 5.58 meV, which shifted to 6.30 meV upon lowering the temperature to 1.5 K. At 300 K, no peak was observed within this energy transition range. Using point charge model calculations, we analysed the crystal electric field effects on the energy levels of the Pr^{3+} magnetic ions. The CEF calculations, performed with the PyCrystalField program, provided an approximate understanding of the CEF environment of the over-stoichiometric $Pr_2NiO_{4.25}$. The calculations showed that the strong peak seen at low temperatures in inelastic neutron scattering experiments comes from two singlets corresponding to the first energy levels of the Pr^{3+} sites without interstitial oxygen. While the first transition for the Pr^{3+} with interstitial as ligand shows an energy much lower, close to the elastic line that barely we could resolve in our scans. Moreover, the calculations revealed a strong link between the position of the first energy transition peak and the Pr-O_{ap} atomic distances.

1. Introduction

Since the discovery of high-temperature superconductivity in $La_2CuO_{4+\delta}$, the impact of oxygen non-stoichiometry on the structure and physical properties of layered oxide compounds was studied extensively. Even slight alterations in oxygen stoichiometry can significantly influence the chemical reactivity and physical properties of these oxides, showing complex structural and electronic behaviours like high-temperature superconductivity, charge and spin ordering, magnetic ordering, spin-dependent transport properties, and multiferroicity [1]. These properties likely rise from the strong interactions between spin, charge, and crystal field effects [2].

Content from this work may be used under the terms of the Creative Commons Attribution 4.0 licence. Any further distribution of this work must maintain attribution to the author(s) and the title of the work, journal citation and DOI.
Published under licence by IOP Publishing Ltd

The Ruddlesden-Popper (RP) series is especially notable for its highly adjustable stoichiometry [3]. This flexibility allows for a wide range of compositions, doping levels, and physical properties. Among these, $RE_2NiO_{4+\delta}$ (*RE* = Pr, La, Nd), with their K_2NiF_4-type structure, have been studied for their structural similarity to the superconducting phase $La_2CuO_{4+\delta}$. While they do not show high-temperature superconductivity, they can accommodate highly mobile excess oxygen, leading to interesting structural, magnetic, and transport features [4].

RE_2NiO_4 structure exhibits a high-temperature tetragonal (HTT) phase across all compositions. As the temperature is reduced, the stoichiometric δ=0 phase undergoes a tilt of the octahedral around the [110] axis, leading to a second-order phase transition to a low-temperature orthorhombic phase (LTO), which is typically observed at room temperature. At even lower temperatures, further tilting around [100] and or [110], results in an additional phase transition to a low-temperature tetragonal or low temperature less orthorhombic structure (LTT)/(LTLO) [5-6].

Compositions with significant excess oxygen ($\sim$ δ=0.25) display an incommensurate structural phase often described by an average orthorhombic *Fmmm* space group [12]. The extra oxygen atoms occupy positions near the (1/4, 1/4, 1/4) interstitial site of the face-centered *2a x 2b x c* RE_2NiO_4 supercell. This interstitial oxygen causes significant displacement of the apical oxygen atoms due to the short O_{ap}-O_{int} distance (approximately 2.15 Å), leading to a symmetrically enlarged $O_{int}(O_{ap})_4$ tetrahedron and complex long-range oxygen ordering [7].

Furthermore, the magnetic properties of $RE_2NiO_{4+\delta}$ are highly sensitive to the incorporation of excess oxygen. In the stochiometric compound the magnetic Ni sublattice orders antiferromagnetically at the Néel temperature T_N=325K. Slight oxygen doping significantly reduces T_N to around 120K for δ=0.25. The oxidation of Ni^{2+} to Ni^{3+} by the excess oxygen causes the competition between ferromagnetic Ni^{2+}-O^{2-}-Ni^{3+} interactions and antiferromagnetic super-exchange Ni^{2+}-O^{2-}-Ni^{2+} and a alteration of long-range magnetic ordering [8]. Opposite to Ni ions that show strong collective dynamics, the magnetic trivalent lanthanide ions (Pr, Nd, La) in these compounds exhibit essentially single-ion characteristics. The local crystal electric field (CEF), which splits the degenerated angular momentum states J of the 4f electrons into a series of energy levels, influences the overall magnetic and physical properties. Understanding the local CEF potentials is essential for gaining insights into the local electronic structure and the ground state of the system.

For the stoichiometric compound $Pr_2NiO_{4.0}$ the low energy CEF excitations were already reported in the literature [9-10]. Studies combining inelastic neutron scattering and heat-capacity experiments have shown that the ground-multiplet of Pr^{3+} splits into five singlets and two doublets due to the electric field created by the surrounding nearest oxygens. The first energy transition is normally reported being around 4.3 meV determined by the separation of the two lowest singlets.

In that case, the CEF environment of the Pr^{3+} ions containing nine close oxygen ligands is commonly described with D_{4h} symmetry. However, because of the tilting of the Ni–O octahedra the actual site symmetry is lower and described by the orthorombic point group D_{2h}. The influence of the distortion due to the shift of the apical oxygens leads to shift in the crystal field levels, showing better agreement with the experimental ones.

The effect of oxygen doping on the CEF environment of this compound has been much less explored so far [11]. In this work, we will present a study of the CEF excitations in $Pr_2NiO_{4.25}$ single crystals. We combine experimental inelastic neutron scattering measurements with point charge

model simulations to describe the crystal electric field environment and establish similarities and differences with respect to the stoichiometric compound.

2. Experiments and methods

2.2 Sample preparation

The single crystal of $Pr_2NiO_{4.25}$ was grown using the traveling solvent floating zone technique, with a NEC SC3-MDH11020 mirror furnace in vertical configuration as described elsewhere [12].

As-grown $Pr_2NiO_{4.25}$ is generally reported to adopt orthorhombic *Fmmm* symmetry, but at ambient temperature it crystallise in a monoclinic structure with the space group $F112/m$ and γ slightly > 90.00°. However, since the monoclinic distortion is extremely small (γ ≈90.03°), the *Fmmm* unit cell remains a good approximation for the theoretical model [13]. Figure 1 shows a schematic representation of the average *Fmmm* cell containing one interstitial oxygen.

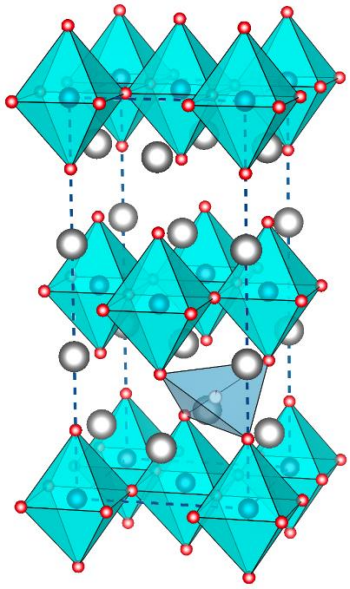


Figure 1. Schematic representation of the $Pr_2NiO_{4.25}$ structure (blue: Ni, red: O, gray: Pr) in the average Fmmm cell containing the interstitial oxygen. O_{int} atom located in the Pr_2O_2 rock salt layer with average occupation of ⅛ and it is tetrahedrally coordinated by the apical oxygen atoms as well as Pr atoms (blue polyhedron).

2.2 Inelastic neutron scattering

The experiments were conducted on the thermal triple-axis spectrometer IN20 at the Institut Laue-Langevin [14]. Both the primary and the second spectrometer employed a monochromatic horizontal and vertical focusing geometry. A sapphire filter window was inserted to reduce the fast neutron background. The incoming and outgoing neutron energies were selected by a doubly focusing PG002 monochromator and a double focusing PG002 analyser, respectively. A fixed final wave-vector k_f = 2. 662 Å^{-1} was used together with a PG002 graphite filter in order to suppress higher order contamination from the monochromator. Several supplemenatry scans have been performed for check on IN8 with a Si111 monochromator, PG002 analyser configuration. The absence of second order scattering due to the diamanod lattice of Si allowed us to disregard any effect due to harmonic contamination [15].

The samples were mounted inside the instrument specific ILL orange cryostats, allowing a temperature range from ambient down to 1.5 K.

2.3 Cristal field calculations

The models for the Pr^{3+} crystal electric field (CEF) excitations were calculated using structural imodels to perform point charge (PC) calculations with the PYCRYSTALFIELD software for Python [16]. The CEF of the system was determined using the Point Charge Model, which serves as an approximation for describing the Hamiltonian given by $\mathcal{H}_{CEF} = -|e|\sum_i V_{CF}(r_i) = \sum_{n,m} B_n{}^m O_n{}^m$, where B are the Stevensons parameters for the crystal field.

3. Results and discussion

For the $Pr_2NiO_{4+\delta}$ compound, containing excess oxygen on the interstitial sites, it is necessary to take in consideration the presence of two different Pr^{3+} environments: one without interstitial oxygen (O_{int}), where 9 ligands are present and which has a local z-axis parallel to the Pr-Oap2 direction (see Fig.2a). The other one considering one O_{int} in addition, we lower the local symmetry by adding one extra oxygen occupying one of the eight possible Wyckoff positions 8f (1/4, 1/4, 1/4) of the respective *Fmmm* unit cell. In this case the previous two-fold symmetry around the local z direction is lost, but a mirror plane passing through O_{int} is preserved, where the local y axis is perpendicular to the (110) mirror plane (Fig.2b).

To carry out the CEF calculation, we selected the *Fmmm* unit cell for theoretical point charge (PC) modelling of the $Pr_2NiO_{4.25}$ crystal. Starting with the *Fmmm* structural model containing one interstitial oxygen (O_{int}) per unit cell, we generated the two sets of Pr-CEF configurations. The first set, which have no O_{int} in their CEF environment, includes 23/4 Pr atoms out of 8 the Pr atoms in the $Pr_2NiO_{4.25}$ unit cell. The second set, which have the O_{int} in their CEF environment, includes 9/4 Pr atoms out of those 8 Pr atoms in the unit cell. This because the O_{int} is shared by the nearby 4 Pr atoms, independent of which Wyckoff position is occupied by O_{int}.

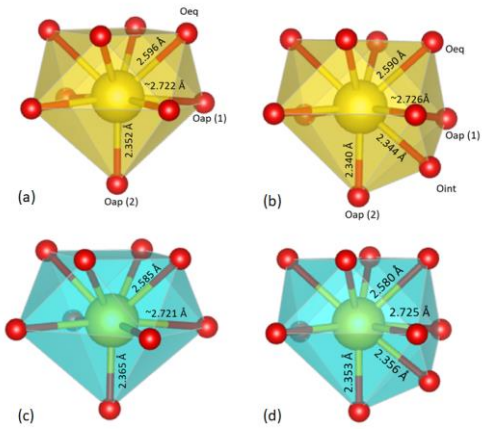


Figure 2. (a) CEF environment of Pr^{3+} ion HT structural model with twofold rotational z axis (b) CEF environment with an extra O_{int} in the HT structure. (c) CEF environment of Pr^{3+} ion LT structural model with twofold rotational z axis (d) CEF environment with an extra O_{int} in the LT structure.

For the set without any interstitial oxygen, thus nine oxygen atoms as ligands, the orthorhombic D_{2h} symmetry allows for only 9 nonzero Stevenson parameters. For the set containing the interstitial oxygen, we applied the lower symmetry (C_{1h}) that maintain a mirror plane along (110) containing the O_{int}. This symmetry choice eliminates the generation of imaginary components and provides us full representation with 15 nonzero Stevensons parameters. Furthermore in order to take into account the effect of temperature on the lattice

parameters and atomic positions within our unit cell, we made the calculations on two theoretical structural models: one for temperatures above 120 K (HT) and another for temperatures below 120 K (LT). These theoretical crystallographic structures result in the four CEF environments depicted in Figure 2, showing both environments with and without interstitial oxygen for both structural models.

Table 1. (a) Calculated CEF parameters from PC model for $Pr_2NiO_{4.25}$ in HT and LT conditions for the Pr^{3+} surrounded by nine oxygen ligands, with charge 2e/O. (b) First two calculated energy levels applying the CEF parameters described in (a). (c) Calculated CEF parameters from PC model for $Pr_2NiO_{4.25}$ in HT and LT conditions for the Pr^{3+} surrounded by ten oxygen ligands, with charge 2e/O. (d) First two calculated energy levels applying the CEF parameters described in (c). [a]$Pr_2NiO_{4.25}$ HT a = 5.3918 Å, b = 5.455 Å, c = 12.44 Å ; [b]$Pr_2NiO_{4.25}$ LT a = 5.3918 Å, b = 5.455 Å, c = 12.38 Å

(a)	Pr^{3+}/ 9_O lig	
B_n^m	[a]$Pr_2NiO_{4.25}$ HT	[b]$Pr_2NiO_{4.25}$ LT
B_2^0	- 1.495	-1.3676
B_2^2	-0.1455	-0.1434
B_4^0	-0.007138	-0.006592
B_4^2	0.002449	0.002478
B_4^4	-0.06069	-0.05928
B_6^0	0.0001378	0.0001351
B_6^2	2.391e-05	2.502e-05
B_6^4	-0.002755	-0.002833
B_6^6	-9.188e-05	9.322e-05

(b)	Pr^{3+}/ 9_O lig E_{calc} (meV)	
Level	[a]$Pr_2NiO_{4.25}$ HT	[b]$Pr_2NiO_{4.25}$ LT
0	0.0	0.0
1	5.78	6.33

(c)	Pr^{3+}/ 10_O lig	
B_n^m	[a]$Pr_2NiO_{4.25}$ HT	[b]$Pr_2NiO_{4.25}$ LT
B_2^0	-3.4637	-3.4521
B_2^1	-8.8367	-8.7173
B_2^2	-2.2584	-2.1276
B_4^0	-0.003505	-0.003405
B_4^1	-0.04739	-0.05017
B_4^2	0.02096	0.02010
B_4^3	-0.1485	-0.1390
B_4^4	-0.008514	-0.007557
B_6^0	0.0002113	0.0001949
B_6^1	0.003621	0.003725
B_6^2	0.0002567	0.0003186
B_6^3	0.002234	0.002210
B_6^4	0.001048	0.001107
B_6^5	-0.001755	-0.001966
B_6^6	0.002160	0.002184

(d)	Pr^{3+}/ 10_O lig E_{calc} (meV)	
Level	[a]$Pr_2NiO_{4.25}$ HT	[b]$Pr_2NiO_{4.25}$ LT
0	0.0	0.0
1	0.28	0.24

The Stevenson parameters of the first set (without Oint, Figure 2a,c) are listed in Table 1(a) for $Pr_2NiO_{4.25}$ in both HT and LT conditions. Utilising those parameters in the CEF Hamiltonian calculation, the 2 lowest energy levels (displayed in Table 1(b)) resemble the ones determined in

the stoichiometric $Pr_2NiO_{4.0}$ compound. This first energy transition, which falls around 6 meV, aligns properly with the experimental observations from INS measurements.

The second set of parameters for the case with the interstitial oxygen and thus a total of 15 non zero Stevenson parameters in both HT and LT condition is presented in Table 1(c). This set results in a CEF Hamiltonian with a distinct energy splitting (Table 1(d)), predominantly producing singlets.

The first excited state calculated within the 10 ligands environment is very close to the ground state, making it difficult to identify this peak in our experimental INS measurements due to its proximity to the zero energy incoherent scattering. Therefore, we assumed that the peak at 6 meV in our INS experiments arises from the CEF environment without the interstitial oxygen, while the one with O_{int} may contribute to the shoulder visible in the low energy side of the main peak (Figure 3). It is still important to take in consideration the second set in order to avoid overestimating the CEF spectral intensity. Consequently, we included both sets in our calculations and performed a weighted sum of the calculated spectra.

Figure 3 shows the results of the CEF calculations and their comparison with experimental CEF from the inelastic neutron scattering experiment at 1.5, 10 and 140K, respectively. The CEF excitation were convoluted with the instrument resolution for proper comparison. We achieved a satisfactory agreement with the experimentally onbserved electronic transition at 140 K (Figure 3c). At lower temperatures, instead, although the peak remains a good approximation of the transition energy, the intensityis less matching, possibly due the Pr magnetically ordering at low temperature that was not included in our calculation.

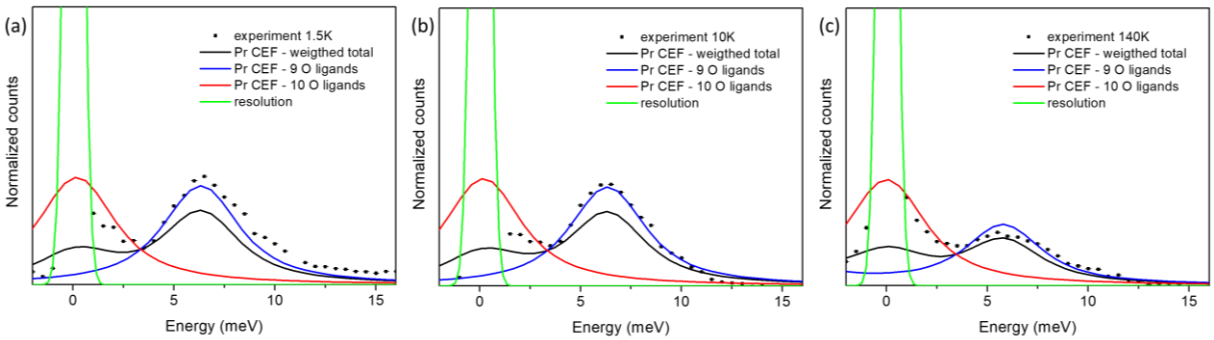


Figure 3. (a) INS spectra of $Pr_2NiO_{4.25}$ measured at the IN20 spectrometer at 1.5 K, with the calculated CEF excitations for the LT model. (b) Same as (a) but at 10 K. (c) INS spectra of $Pr_2NiO_{4.25}$ measured at the IN20 spectrometer at 140 K, along with the calculated CEF excitations for the HT model. For all plots, black scatter are experimental data, green line is the instrument resolution, blue line is the CEF from Pr ions with 9 ligands, red line is CEF from Pr ions with 10 ligands, black line is the weighted sum.

We found that the point charge model provides a good approximation for the first two electronic states of the Pr^{3+} CEF environment. It is evident that the Pr^{3+} configuration without interstitial oxygen gives rise to the strong energy transition around 6 meV. This transition is found experimentally and theoretically with the applied model for oxygen-doped compounds, similarly to the stoichiometric case. Still, we observe a difference in energy of 1.37 meV between $Pr_2NiO_{4.0}$ and $Pr_2NiO_{4.25}$ at 140 K and 2.1 meV between $Pr_2NiO_{4.0}$ and $Pr_2NiO_{4.25}$ at 10 and 1.5 K.

To point out where the energy shifts come from, we need to have a look on two effects affecting the Pr^{3+} environment, the presence of the interstitial oxygen and the changes of the oxygen position with temperature. As a matter of fact, the oxygen doping has a strong impact on both the *c* lattice parameter and on the relative atomic positions of the Pr atoms and apical

oxygens. This means that O_{int} introduction impacts to a larger extent the bond length Pr-O_{ap} of the Pr^{3+} sites, impact that extend also to the Pr-Oap bond lengths away from O_{int} site. Instead, changes due to temperature are mostrly related to the variation of the *c* axis only. with a reduced impact on the atomic distances between Pr and the apical oxygens.

Using a set of calculations based on the point charge model for a Pr^{3+} ion surrounded by nine oxygen ligands, we observed an exponential dependence between the Pr-O_{ap} distances and the crystal electric field (CEF) energy levels. The plots shown in Figure 4 clearly demonstrate that the calculated energy transition is highly sensitive to the Pr-O_{ap} distances. Specifically, for the Pr-O_{ap1} bond shorter is the distance higher the CEF transition is expected (red squares, Figure 4). Opposite to this , for the Pr-O_{ap2} bond longer is the distance higher the CEF transition is expected (black squares, Figure 4).

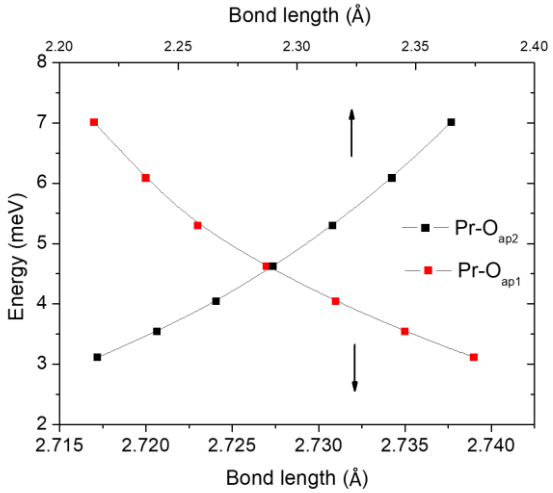


Figure 4. Trend of first CEF level energy obtained through point charge model calculations by varying the atomic positions of O_{ap}. Red squares are connected to the Pr-O_{ap1} bond length, black squares to the Pr-O_{ap2} bond length as defined in Figure 2.

It is important to emphasise that the point charge model is primarily useful for providing information on relative changes in the crystal electric field (CEF); an absolute calculation would need to include the effects of further neighbours, screening, and bond delocalization. Moreover, it should be noted that PyCrystalField does not include the exchange interaction in the Hamiltonian. In numerous magnetic systems, also the exchange interaction between magnetic ions has to be taken into account. Above 40 K, Pr ions are paramagnetic in our compound and calculation should be sufficiently accurate, but below this temperature their magnetic moments are probably coupled to the Ni sublattices. This might also be the reason for the larger discrepancies in the comparison of model with experimental data. Consequently we indirectly found that, at such lower temperatures, exchange interactions involving these magnetic ions have an influence our CEF environment that wil have to be explored further.

4. Conclusions

In this study, we investigated the crystal electric field (CEF) excitations of $Pr_2NiO_{4.25}$ using inelastic neutron scattering data combined with point charge model calculations.

Energy scans at three different temperatures reveal the low-energy excitation peaks for $Pr_2NiO_{4.25}$: 5.58 meV at 140 K and 6.30 meV at 10 K and 1.5 K. At 300 K. Any clear peak could be

observed within this first energy transition range of Pr ion environment conatining O_{int}, but a shoulder at corresponding energy exist.

For $Pr_2NiO_{4.25}$ a point charge model for to two sets of Pr^{3+} CEF environments (with and without interstitial oxygen) could reproduce the strong low-energy CEF excitation peak observed in the 0 - 15 meV range of the INS spectrum. The calculations suggested that the first strong peak in our experimental data primarily arises from the first energy transition in the CEF environment without extra oxygen, with the interstitial oxygen set contributing mainly to the peak's intensity while marginally on the shoulder.

Identifying the peak from the CEF environment with interstitial oxygen in our INS measurements was challenging due to its proximity to the zero-energy incoherent scattering. Nevertheless, we achieved a very satisfactory agreement with the CEF first electronic transition at 140 K. At lower temperatures, although the peak's energy transition approximation remained good, the intensity did not match as well, possibly as consequence of Pr/O_{int} ordering at low temperatures, which is not included in the point charge model calculations.

The point charge model calculations also indicated a strong correlation between the first energy transition peak position and the $Pr\text{-}O_{ap}$ atomic distances.

A more precise calculation would need to include additional effects present in the material. In particular, for a better calculation of our CEF environment at low temperatures, we need to incorporate the exchange interaction.

Acknowledgements

Part of this work was funded by a collaborative international research project “ExODiff” between the French National Research Agency (ANR-19-CE05-0041) and the Deutsche Forschungsgemeinschaft (DFG ME-3488/2-1).

References

[1] H. Ulbrich, M. Braden 2012 Physica C **481** 31-45
[2] E. Dagotto, 1994 Reviews of Modern Physics **66**(3) 763-840.
[3] P. D. Battle, C. W. Jones 1989 Journal of Solid State Chemistry **78**(1) 108-119.
[4] L. Minervini, R. W. Grimes, J. A. Kilnera, K. E. Sickafus 2000 Material Cheistry **10** 2349-2354.
[5] C. Allançon, A. Gonthier-Vassal, J.M. Bascat, J.P. Loup, P. Odier 1994 Solid State Ionics **74**(3–4) 239-248.
[6] W. Paulus, et al. 2002 Solid State Sciences **4**(5) 565-573.
[7] M. Ceretti, et al. 2015 Journal of Material Chemistry A **3** 21140-21148.
[8] S. R. Maity, et al. 2021 Phys. Rev. Materials **5** 014401.
[9] A. T. Boothroyd, et al. 1997 Journal of Physics.: Condensed Matter **9** 2275.
[10] M. Castro et al. 1997 Physica B **234-236** 728-730.
[11] R Dutta et al. 2022 Physical Review B **105** 195147.
[12] O. Wahyudi et al. 2015 CrystEngComm **17** 6278-6285.
[13] R. Dutta, et al. 2020 Journal of Material Chemistry A **8** 13987-13995.
[14] http://dx.doi.org/10.5291/ILL-DATA.4-01-1800
[15] http://dx.doi.org/10.5291/ILL-DATA.TEST-3383
[16] A. Scheie 2021 Applied Crystallograpy **54** 356.